HHS Public Access

Author manuscript

Bioconjug Chem. Author manuscript; available in PMC 2017 February 03.

Published in final edited form as:

Bioconjug Chem. 2016 June 15; 27(6): 1447–1455. doi:10.1021/acs.bioconjchem.5b00679.

Preclinical Comparative Study of ^{68}Ga-Labeled DOTA, NOTA, and HBED-CC Chelated Radiotracers for Targeting PSMA

Sangeeta Ray Banerjee[*], **Zhengping Chen**, **Mrudula Pullambhatla**, **Ala Lisok**, **Jian Chen**, **Ronnie C. Mease**, and **Martin G. Pomper**[*]

Russell H. Morgan Department of Radiology and Radiological Science, Johns Hopkins Medical Institutions, Baltimore, Maryland 21287, United States

Abstract

^{68}Ga-labeled, low-molecular-weight imaging agents that target the prostate-specific membrane antigen (PSMA) are increasingly used clinically to detect prostate and other cancers with positron emission tomography (PET). The goal of this study was to compare the pharmacokinetics of three PSMA-targeted radiotracers: ^{68}**Ga-1**, using DOTA-monoamide as the chelating agent; ^{68}**Ga-2**, containing the macrocyclic chelating agent *p*-SCN-Bn-NOTA; and ^{68}Ga-DKFZ-PSMA-11, currently in clinical trials, which uses the acyclic chelating agent, HBED-CC. The PSMA-targeting scaffold for all three agents utilized a similar Glu-urea-Lys-linker construct. Each radiotracer enabled visualization of PSMA+ PC3 PIP tumor, kidney, and urinary bladder as early as 15 min post-injection using small animal PET/computed tomography (PET/CT). ^{68}**Ga-2** demonstrated the fastest rate of clearance from all tissues in this series and displayed higher uptake in PSMA+ PC3 PIP tumor compared to ^{68}**Ga-1** at 1 h post-injection. There was no significant difference in PSMA+ PC3 PIP tumor uptake for the three agents at 2 and 3 h post-injection. ^{68}Ga-DKFZ-PSMA-11 demonstrated the highest uptake and retention in normal tissues, including kidney, blood, spleen, and salivary glands and PSMA-negative PC3 flu tumors up to 3 h post-injection. In this preclinical evaluation ^{68}**Ga-2** had the most advantageous characteristics for PSMA-targeted PET imaging.

Graphical abstract

[*]**Corresponding Authors** sray9@jhmi.edu. Phone: 410-955-8697. Fax: 410-614-3147. [*] mpomper@jhmi.edu. Phone: 410-955-2789. Fax: 443-817-0990.

Supporting Information

The Supporting Information is available free of charge on the ACS Publications website at DOI: 10.1021/acs.bioconjchem.5b00679.

Comparison of PSMA+ PC3 PIP tumor to PSMA-negative flu tumor and selected tissues for the agents and ^{1}H NMR, preparative HPLC chromatograms for ^{68}**Ga-1**, ^{68}**Ga-2**, and ^{68}Ga-PSMA-11 (PDF)

The authors declare no competing financial interest.

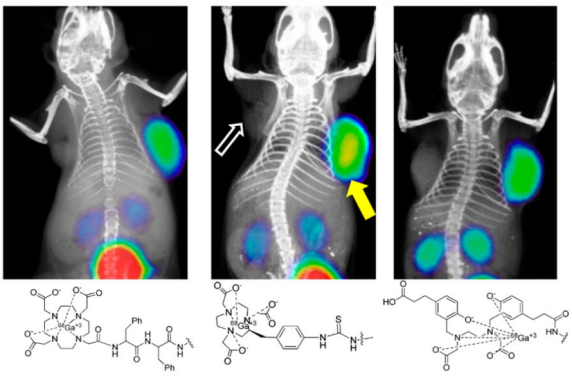

INTRODUCTION

According to the National Cancer Institute, approximately 220 800 cases of prostate cancer will be diagnosed in 2015 in the U.S., with over 27 540 proving lethal (~12.5%).[1] Existing imaging techniques for detection and therapeutic monitoring of prostate cancer are inadequate for effective management of the disease. The transmembrane glycoprotein prostate-specific membrane antigen (PSMA) is increasingly recognized as an important target for both imaging and therapy of prostate cancer.[2,3] PSMA is found in benign as well as in malignant prostate tissue.[4–6] However, expression of PSMA is greatest in prostate adenocarcinoma, particularly in castration-resistant disease.[7,8] PSMA is also present in the neovasculature of solid tumors including kidney, lung,[9] stomach, colon, and breast.[10–12] Expression of PSMA is associated with the neovascular endothelium in nonprostate tumors.[13,14]

We and others have used PSMA-targeted agents to image patients with prostate cancer using positron emission tomography (PET).[15–21] Although there are debatable advantages and disadvantages with respect to which isotope to use for detection with PET, namely, ^{18}F vs ^{68}Ga, the radiometal ^{68}Ga can be produced on-site with a generator, followed by simple synthesis of the radiotracer.[22] We previously reported ^{68}**Ga-1**, a radiotracer that employed the DOTA-monoamide chelator with conjugation to H_2N-Lys-$(CH_2)_3$-Lys-urea-Glu for targeting to PSMA (Figure 1).[23] We chose that chelator to make it possible to complex imaging radiometals, such as ^{68}Ga, ^{86}Y, or ^{203}Pb, as well as therapeutic radiometal nuclides, such as ^{177}Lu, ^{90}Y, ^{212}Pb, or ^{225}Ac, within the same scaffold. Since then, two ^{68}Ga-based agents have demonstrated excellent clinical results for detection of prostate cancer, namely, ^{68}Ga-DKFZ-PSMA-11 (Glu-urea-Lys-(Ahx)-HBED-CC) and EuK-Subkff-^{68}Ga-DOTAGA (^{68}Ga-PSMA I&T).[24–27] Those compounds both employ the Glu-Lys-urea-based PSMA-targeted moiety, while ^{68}Ga-DOTA-DUPA-Pep, also recently tested clinically, uses DOTA-monoamide as the chelating agent and Glu-Glu-urea as the PSMA-targeting moiety.[28] A recent preclinical study also evaluated ^{68}Ga-(CHX-A″-DTPA)-Pep using CHX-A″-DTPA as the chelating agent.[29] Among the agents, ^{68}Ga-DKFZ-PSMA-11 has been most widely studied clinically.[2,16–18,30,31]

Due to the growing number of clinical trials employing ^{68}Ga-based, PSMA-targeted PET, we decided to investigate structural elements that could promote the least off-target uptake

of this class of radiotracers. Specific attention was given to decreasing activity within renal and salivary gland tissue, commonly seen with these agents. Here we describe a head-to-head, preclinical comparison of ^{68}**Ga-1**, ^{68}**Ga-2**, a new radiotracer containing the macrocyclic chelating agent NOTA, and ^{68}Ga-DKFZ-PSMA-11. Tumor uptake, selectivity, and pharmacokinetics were assessed. Although we would prefer head-to-head studies in clinical subjects, we believe that a preclinical study such as this retains value as it is carefully controlled and all of the aforementioned agents were evaluated for pharmacokinetics in preclinical studies[23,24]—with similar comparisons performed—before their successful move to the clinic.[24,25]

RESULTS

Chemical and Radiochemical Syntheses and Characterization

Structures of the radioligands used for the study are shown in Figure 1. Lys-Glu urea was used as the PSMA-targeting moiety in all cases. Selected physical properties of **1**, **2**, and the corresponding natural Ga-complexes are summarized in Table 1. Since NOTA is a hexadentate N_3O_3 macrocyclic chelator, ^{68}Ga-**2** was expected to produce a neutral compound.[32] DKFZ-PSMA-11 chelated with HBED-CC is reported to provide a uninegative, hexadentate chelation (N_2O_4) to Ga(III) at room temperature, with two carboxylates and two phenolates.[33–35] All three radiotracers were synthesized in high radiochemical yield (~95–99%) and purity (>98%), with specific radioactivity >168 GBq/μmol (4.05 mCi/μmol).

We have investigated two radiolabeling methods, one in the presence of HEPES buffer as reported by Eder et al.[24] and the other by a method reported by us[23] following a literature procedure.[36] For the latter method, preconcentrated ^{68}Ga(III)-Cl_3 could be directly used for radiolabeling, without adjusting pH, and radiolabeling could be done in a total volume of 300–350 μL using as low as 4 μg of any of the three ligands. Based on the HPLC retention time (Table 1), the nonradiolabeled precursor DKFZ-PSMA-11 was the least hydrophilic, although, after radiolabeling, ^{68}Ga-DKFZ-PSMA-11 became the most hydrophilic compound in the series. The partition coefficient (log *P*) between *n*-octanol and PBS was also determined. Both ^{68}**Ga-2** (−4.04 ± 0.16) and ^{68}Ga-DKFG-PSMA-11 (−3.89 ± 0.16) were found to be 1 order of magnitude more hydrophilic than ^{68}**Ga-1** (−3.0 ± 0.1).

Precursor ligands and the corresponding stable metal-labeled compounds demonstrated high binding affinity to PSMA, with K_i values ranging from 0.03 to 0.81 nM (Table 1). The known, high-affinity PSMA inhibitor ZJ43[37] was used as a reference ligand and exhibited a K_i of 0.31 nM (Table 1). DKFZ-PSMA-11 displayed the highest PSMA-binding affinity from the compounds tested in this comparative study.

Cellular Uptake and Internalization Studies

Comparative cell uptake and internalization experiments using isogenic human prostate cancer PSMA+ PC3 PIP and PSMA− PC3 flu cells revealed significantly higher uptake and internalization of ^{68}**Ga-2** and ^{68}Ga-DKFZ-PSMA-11 compared to ^{68}**Ga-1** as shown in Figure 2. The HBED-CC conjugate ^{68}Ga-DKFZ-PSMA-11 demonstrated significantly

higher cell surface uptake and internalization at 30 and 60 min post-incubation compared to ^{68}**Ga-1** ($P < 0.001$ for both cell lysate and glycine wash) and for ^{68}**Ga-2** ($P < 0.001$ glycine wash at 30 and 60 min and cell lysate at 60 min $P < 0.05$) from the series. Cell uptake of the three agents can be specifically blocked nearly completely with excess ZJ43 (10 μM). For all three agents there was a fast cell internalization rate from 10 to 30 min with a slow rate of internalization noted from 30 min to 1 h post-incubation at 37 °C.

Biodistribution

Table 2 shows the pharmacokinetics in selected organs for ^{68}**Ga-1**, ^{68}**Ga-2**, and ^{68}Ga-DKFZ-PSMA-11, respectively. All compounds exhibited clear PSMA-dependent binding in PSMA+ PC3 PIP tumor xenografts. The tumor uptake for ^{68}**Ga-1** was 19.5 ± 1.8% ID/g at 1 h, highest at 2 h (24.8 ± 1.1% ID/g), and remained high at 3 h post-injection (19.5 ± 5.1% ID/g) (Table 2). PSMA+ PC3 PIP-to-PSMA-PC3 flu tumor uptake ratios were 84 ± 4 at 1 h and 149 ± 16 at 2 h. The distribution within normal organs and tissues was also favorable, with low blood and normal tissue uptake and rapid clearance. The highest accumulation of radioactivity was observed in the kidneys, where uptake was expectedly high and peaked at 26.5 ± 6.9%ID/g at 1 h and decreased to 11.9 ± 1.0%ID/g by 2 h and remained roughly the same at 3 h post-injection.

^{68}**Ga-2** showed the highest PSMA-dependent tumor uptake with 42.2 ± 6.7%ID/g at 1 h post-injection. Tumor uptake remained high, with faster clearance from 1 to 2 h. The PSMA + PC3 PIP-to-PSMA− PC3 flu tumor ratios were 110 ± 22 at 1 h, 232 ± 26 at 2 h, and 182 ± 15 at 3 h. Renal uptake for ^{68}**Ga-2** was highest at 1 h, 106 ± 23%ID/g, much higher than that seen for ^{68}**Ga-1**, and showed faster renal clearance, which decreased to 34.7 ± 5.7%ID/g by 2 h post-injection. In addition, nontarget organs, such as blood, heart, liver, spleen, stomach, and pancreas, showed lower uptake (≤1%ID/g at 1 h, except for spleen) and faster clearance than for ^{68}**Ga-1**.

^{68}Ga-DKFZ-PSMA-11 showed the highest PSMA-dependent tumor uptake with 26.9 ± 5.6% ID/g at 3 h post-injection. Tumor uptake was nearly comparable from 1 to 3 h post-injection. The PSMA+ PC3 PIP-to-PSMA− PC3 flu ratios were 47 ± 8 % at 1 h, 58 ± 27 at 2 h, 164 and 111 ± 21 at 3 h post-injection.

Figure 3 summarizes several comparative tissue uptake properties of the three agents. PSMA + PC3 PIP tumor uptake of ^{68}**Ga-2** was significantly higher than ^{68}**Ga-1** at 1 h post-injection ($P < 0.01$) (Figure 3A). There was no significant difference in PSMA+ PIP tumor uptake between ^{68}**Ga-1** and ^{68}Ga-DKFZ-PSMA-11 or between ^{68}**Ga-2** and ^{68}Ga-DKFZ-PSMA-11 ($P > 0.05$) at any time-point. As shown in Figure 3B, renal uptake of ^{68}**Ga-1** was significantly lower than ^{68}**Ga-2** and ^{68}Ga-DKFZ-PSMA-11 ($P < 0.001$) at 1 h, although there was no significant difference between ^{68}**Ga-2** and ^{68}Ga-DKFZ-PSMA-11.

At 2 h post-injection renal uptake of both ^{68}**Ga-1** and ^{68}**Ga-2** were significantly lower than for ^{68}Ga-DKFZ-PSMA-11 ($P < 0.001$) and renal uptake of ^{68}**Ga-1** was still significantly lower than ^{68}**Ga-2** ($P < 0.01$). At 3 h post-injection renal uptake of both ^{68}**Ga-1** and ^{68}**Ga-2** was significantly lower than for ^{68}Ga-DKFZ-PSMA-11 ($P < 0.001$). Figure 3C reveals that ^{68}Ga-DKFZ-PSMA-11 demonstrated significantly higher salivary gland uptake up to 3

h after injection compared to ^{68}**Ga-1** and ^{68}**Ga-2** ($P < 0.001$). Figure 3D shows higher spleen uptake for ^{68}Ga-DKFZ-PSMA-11 compared to either ^{68}**Ga-1** or ^{68}**Ga-2** at all time-points. Between ^{68}**Ga-1** and ^{68}**Ga-2**, the former showed significantly lower spleen ($P < 0.05$) uptake at 1 and 2 h post-injection compared to the latter. Selected PSMA+ PC3 PIP tumor-to-background for the three agents at 1–3 h post-injection are shown in Supporting Information Figure S1. As anticipated from the biodistribution data, PSMA+ PC3 PIP tumor-to-salivary gland ($P < 0.001$) and PSMA+ PC3 PIP tumor-to-kidney ratios proved significantly higher for ^{68}**Ga-1** and ^{68}**Ga-2** than for ^{68}Ga-DKFZ-PSMA-11 ($P < 0.001$).

PSMA+ PC3 PIP tumor-to-PSMA− PC3 flu tumor ratios were also significantly higher for ^{68}**Ga-1** and ^{68}**Ga-2** compared to ^{68}Ga-DKFZ-PSMA-11 at 1 h post-injection ($P < 0.001$). The data show that PSMA+ PC3 PIP tumor-to-blood ratios were highest for ^{68}**Ga-2** at all three time points.

Small Animal PET-CT Imaging

Whole body PET-CT images were studied for ^{68}**Ga-1**, ^{68}**Ga-2**, and ^{68}Ga-DKFZ-PSMA-11 in intact male NOD/SCID mice (Figure 4) bearing both PSMA+ PC3 PIP and PSMA− PC3 flu xenografts in opposite, upper flanks. Irrespective of charge and lipophilicity, all radiotracers enabled visualization of PSMA+ PC3 PIP tumor and kidneys (Figure 4). As anticipated from the biodistribution results, for all three agents PSMA+ PC3 PIP tumor was visible as early as 15 min post-injection. Renal uptake of the radiotracers is partially due to the route of excretion of these agents as well as to specific uptake from the expression of PSMA in mouse proximal renal tubules.[8] All three agents showed significant bladder activity, indicating rapid renal clearance. A reduction of the tumor and kidney uptake to background levels was observed with the blocking agent ZJ43 for ^{68}**Ga-2**, indicating PSMA-mediated accumulation. The results of blocking studies are in agreement with our previous report for ^{68}**Ga-1** using ZJ43[23] and for PSMA-11 by Eder et al.[24] using 2-phosphonomethyl pentanedioic acid (2-PMPA).

DISCUSSION

Structural optimization of low-molecular-weight imaging and therapeutic agents targeting PSMA is under active investigation.[23,38–48] Such optimization is geared toward high tumor uptake with minimal off-target, namely, renal and salivary gland, uptake at times convenient for imaging and endoradiotherapy. High salivary gland uptake in particular has proven to be a concern. We originally synthesized ^{68}**Ga-1**, [23] with the DOTA chelator to enable imaging or therapy, depending on the radionuclide employed. We previously showed that a linker to DOTA containing a *p*-isothiocyanatobenzyl function provided the most suitable pharmacokinetics in a small series of compounds generated for imaging PSMA with ^{86}Y-PET.[48] NOTA has been shown to be an effective chelating agent for ^{68}Ga (stability constant, $K_{ML} = 31.1$), compared to DOTA ($K_{ML} = 21.3$).[49,50] We used the commercially available *p*-isothiocyanatobenzyl derivative of NOTA in ^{68}**Ga-2** for its mild radiolabeling conditions in the hope of creating a ^{68}Ga-based agent with improved pharmacokinetics that could be generated simply, as in a kit-like preparation at room temperature. We compared the in vivo

performance characteristics of ^{68}**Ga-1**, ^{68}**Ga-2**, and ^{68}Ga-DKFZ-PSMA-11, the latter of which has been used throughout Europe in clinical trials.

To improve precision with respect to the comparison, all three radiotracers were purified by HPLC to remove unlabeled ligand. The results obtained from biodistribution and imaging experiments indicated that there were no differences in absolute uptake among the three agents in PSMA-expressing tumors (Figure 2 and Supporting Information Figure S1), except for higher uptake for ^{68}**Ga-2** at 1 h post-injection ($P < 0.007$ between ^{68}**Ga-2** and ^{68}**Ga-1**). That lack of difference was despite the 5-fold lower degree of internalization of ^{68}**Ga-1** than for ^{68}**Ga-2** or ^{68}Ga-DKFZ-PSMA-11 (Figure 2). Internalization, believed to be a key element for a successful radiotherapeutic, may be less important for detection and imaging, at least under the conditions of the current study. We found higher nonspecific uptake for ^{68}Ga-DKFZ-PSMA-11 than for ^{68}**Ga-1** or ^{68}**Ga-2**, contrary to Eder et al.,[24] in which ^{68}**Ga-1** was compared to ^{68}Ga-DKFZ-PSMA-11 (Figure 2 and Supporting Information Figure S1). We believe that discrepancy derived from the lack of HPLC purification for ^{68}**Ga-1** in Eder et al.,[24] which could negatively impact its effective specific activity. Another possibility could be the different tumor models used, with LNCaP used in the earlier report,[24] and PSMA+ PC3 PIP for the PSMA-expressing positive control. However, we have previously reported that the level of expression of PSMA in PSMA+ PC3 PIP tumors was very similar to that in LNCaP.[51]

As has been previously shown by us and others in the field of PSMA imaging with low-molecular-weight agents,[24,25,28,46,48,52,53] the key parameter of nonspecific tissue uptake depends on the overall physicochemical properties of the radiolabeled agent, including the metabolic stability of the metal-chelate complex, charge, and lipophilicity. Both the chelating agent and the linker employed to attach the radionuclide to the targeting agent are important in establishing those physicochemical features—particularly for compounds <1500 Da. For example, we have shown that certain ^{99m}Tc-oxo cores with different combinations of N_xS_y-based chelating agents demonstrated high retention in kidney and spleen for more than 6 h.[45] Such agents displayed high PSMA+ tumor retention. On the other hand, ^{99m}Tc(CO)$_3$-based agents showed much faster clearance from most normal tissues including kidneys, although, these agents showed slightly higher gastrointestinal uptake at initial time-points (<2 h). We have also observed high kidney uptake and retention for NOTA-chelated ^{64}Cu-labeled PSMA-inhibitor compared to the CB-TE2A-conjugated ^{64}Cu-labeled agent[46] although both chelating agents are known to form a copper complex with comparable stability.[54,55] Modifying linker and chelating agent indeed revealed significant changes in biodistribution pattern as recently reported by Eder et al.[47] A preclinical comparison of DOTA-mono amide chelated PSMA-targeting agent, ^{68}Ga-DKFZ-PSMA-617 vs HBED-CC-conjugated ^{68}Ga-DKFZ-PSMA-11 demonstrated higher tumor uptake at later time points, lower spleen accumulation, and fast clearance of radioactivity from the kidneys for the DOTA-chelated agent.

CONCLUSION

We report a preclinical comparative study to evaluate the in vivo pharmacokinetics of three ^{68}Ga-labeled PSMA-targeting PET radiopharmaceuticals. The macrocyclic NOTA

chelated agent ^{68}**Ga-2** demonstrated the highest PSMA+ tumor accumulation at clinically convenient times post-injection, and showed rapid clearance from most normal tissues, including kidney and salivary gland. ^{68}**Ga-2** is a clinically viable imaging agent for detecting PSMA+ lesions.

EXPERIMENTAL PROCEDURES

Solvents and chemicals purchased from commercial sources were of analytical grade or better and used without further purification. [^{68}Ga]$GaCl_3$ was obtained from the University of Wisconsin. DOTA-tris(*t*-butyl ester)-monoacid and *p*-SCN-Bn-NOTA were purchased from Macrocyclics, Inc. (Dallas, TX). Compounds **1** and **2** were synthesized following our previous reports.[23,46] DKFZ-PSMA-11 and the corresponding stable Ga-DKFZ-PSMA-11 were purchased from ABX (Radeberg, Germany). Triethylsilane (Et_3SiH), diisopropylethylamine (DIEA), and triethylamine (TEA) were purchased from Sigma-Aldrich (St. Louis, MO). All other chemicals were purchased from Thermo Fisher Scientific (Pittsburgh, PA) unless otherwise specified.

Analytical thin-layer chromatography (TLC) was performed using Aldrich aluminum-backed 0.2 mm silica gel Z19, 329-1 plates and was visualized by ultraviolet light (254 nm), I_2, and 1% ninhydrin in EtOH. Flash chromatography was performed using silica gel (MP SiliTech 32–63 D 60 Å) purchased from Bodman (Aston, PA). All in vitro PSMA binding studies and determination of partition coefficients were performed in triplicate to ensure reproducibility, as previously reported. ^{1}H NMR spectra were recorded on a Bruker Ultrashield 400 MHz spectrometer. Chemical shifts (δ) are reported in ppm downfield in reference to proton resonances resulting from incomplete deuteration of the NMR solvent. Quantitative ^{1}H NMR was used to prove that all synthesized compounds were at >95% chemical purity.

Low resolution ESI mass spectra were obtained on a Bruker Daltonics Esquire 3000 Plus spectrometer. High resolution mass spectra were obtained by the University of Notre Dame Mass Spectrometry & Proteomics Facility, Notre Dame, IN, using electrospray ionization (ESI) mass spectrometry either by direct infusion on a Bruker microTOF-II or by LC elution via an ultra-high-pressure Dionex RSLC C_{18} column coupled to a Bruker microTOF-Q II. The purity of tested compounds was also determined by analytical high performance liquid chromatography (HPLC) with absorbance at 220 nm and were all again determined to be >95%.

HPLC purification of stable compounds was performed using a Phenomenex C_{18} Luna 10 × 250 mm^2 column and elution with water (0.1% TFA) (A) and CH_3CN (0.1% TFA) (B) on a Waters 600E Delta LC system with a Waters 486 variable wavelength UV/vis detector, both controlled by Empower software (Waters Corporation, Milford, MA). HPLC purifications of ^{68}**Ga-1**, ^{68}**Ga-2**, and ^{68}Ga-DKFZ-PSMA-11 were performed on a Varian Prostar System (Palo Alto, CA), equipped with a Varian ProStar 325 UV–vis variable wavelength detector and a Bioscan Flow-count in-line Radioactivity detector (Washington, DC., all controlled by Galaxie software (Varian Inc., Walnut Creek, CA).

All radiotracers were purified using a Varian microsob-MV 100-5 C_8 25 × 4.6 mm column with a flow rate 1 mL/min with water (0.1% TFA) (A) and CH_3CN (0.1% TFA) (B) as the eluting solvents. In order to ensure uniform purity of the compounds undergoing comparison, various HPLC methods were applied to separate excess ligand from the radiolabeled compound. For ^{68}**Ga-1**, an isocratic solution of 80% A and 20% B was used. For ^{68}**Ga-2** and ^{68}Ga-DKFZ-PSMA-11, an isocratic solution of 85% water and 15% B was employed.

Retention times of the radiolabeled compound and unlabeled free ligands are listed in Table 1. The radiochemical yield and purity of the radiotracers were further checked by withdrawing 1 μL aliquots of the radiolabeled solution and were analyzed by radio-TLC on RP-18 thin layer plates using 5/1 saline/ methanol as the mobile phase. The specific radioactivity was calculated as the radioactivity eluting at the retention time of product during the preparative HPLC purification divided by the mass corresponding to the area under the curve of the UV absorption.

Radiolabeling Methods

^{68}Ga-Labeling of target ligands was performed according to our previously reported method[23] and following other literature procedures.[24,36] Briefly, 488 MBq (13 mCi) of $^{68}GaCl_3$ in 7 mL of 0.1 N HCl were obtained from an 18-month-old 1850 MBq (50 mCi) ^{68}Ge/^{68}Ga generator, Eckert-Ziegler (Berlin, DE). Preconcentration was performed on a cation-exchange cartridge. The purified $^{68}Ga(III)Cl_3$ was obtained in a total volume of 400 μL, eluted in 2.4/97.6 0.05 N HCl/acetone. The ^{68}Ga(III) in HCl/acetone was used immediately for the radiolabeling of **1, 2**, or DKFZ-PSMA-11.

We investigated two radiolabeling techniques. The first was undertaken in water (without any added buffer solution), as we reported earlier,[23] and the second used 2.1 M HEPES buffer at pH ~ 4, as reported by Eder et al.[24] Using HEPES buffer, each ligand (12.5 μg), was radiolabeled in >95% yield in a total volume of ~120 μL; however, the yield was dependent on the total volume of the radiolabeling solution. In water the preconcentrated $^{68}Ga(III)Cl_3$ solution could be directly used for radiolabeling at pH ~ 3–4.[23] The total volume of the radiolabeling solution was ~300–350 μL to produce >93% yield using ~4–6 μg of each precursor ligand.

In a typical reaction 50 μL of the concentrated radioactivity was added to 250 μL of deionized H_2O in a 1.5 mL polypropylene vial, followed by addition of 3–5 μL of a solution of precursor ligand (2 μg/μL in water, pH ~ 3.5–4). The reaction vial was heated at 95 °C for 10 min for ligand **1**, ~3 min for ligand **2**, and the complex was allowed to form at room temperature for 10 min for both **2** and DKFZ-PSMA-11. Complex formation was monitored by iTLC as above, using 5/ 1 saline/methanol.

For the comparison studies, all three radiotracers were purified by HPLC to remove excess precursor ligand so that all three radioligands could be obtained in >98% purity. The acidic eluate was neutralized with 50 μL 1 M Na_2CO_3 and the volume of the eluate was reduced under vacuum to dryness. The solid residue was diluted with saline to the desired radioactivity concentration for biodistribution and imaging studies.

PSMA Inhibition Assay

The PSMA inhibitory activity of **1**, **2**, and DKFZ-PSMA-11 and the corresponding natural Ga-labeled analogues **Ga-1** and **Ga-2** were determined using a fluorescence-based assay according to a previously reported procedure (Table 1).[51] Briefly, lysates of LNCaP cell extracts (25 μL) were incubated with the inhibitor (12.5 μL) in the presence of 4 μM *N*-acetylaspartylglutamate (NAAG) (12.5 μL) for 2 h. The amount of the glutamate released by NAAG hydrolysis was measured by incubating with a working solution (50 μL) of the Amplex Red Glutamic Acid Kit (Life Technologies, Grand Island, NY) for 1 h.

Fluorescence was measured with a VICTOR3 V multilabel plate reader (PerkinElmer Inc., Waltham, MA) with excitation at 490 nm and emission at 642 nm. Inhibition curves were determined using semilog plots and IC_{50} values were determined at the concentration at which enzyme activity was inhibited by 50%. Enzyme inhibitory constants (K_i values) were generated using the Cheng-Prusoff conversion.[56] Assays were performed in triplicate. Data analysis was performed using GraphPad Prism v 4.00 for Windows (GraphPad Software, San Diego, California).

Determination of Lipophilicity

To a solution of 0.5 to 1 MBq of each ^{68}**Ga-1**, ^{68}**Ga-2**, and ^{68}Ga-DKFG-PSMA-11 in 3 mL of phosphate-buffered saline (PBS, pH 7.4), was added 3 mL of *n*-octanol ($n = 3$) in 15 mL Eppendorf tubes. At ambient temperature tubes were vortexed vigorously for 3 min and were centrifuged at 3000 *g* for 5 min. The activity concentrations in 100 μL samples of both the aqueous and the organic phases were measured in a γ-spectrometer (1282 Compugamma CS; Pharmacia/LKB Nuclear, Inc., Gaithersberg, MD). The partition coefficient was calculated as a ratio between counts in the *n*-octanol phase to counts in the water phase.

Cell Lines

Sublines of the androgen-independent PC3 human prostate cancer cell line, originally derived from an advanced androgen-independent bone metastasis, were used. Those sublines have been modified to express high levels of PSMA [PSMA-positive (+) PC3 PIP] or are devoid of target [PSMA-negative (−) PC3 flu]. They were generously provided by Dr. Warren Heston (Cleveland Clinic). Cells were grown in RPMI 1640 medium (Corning Cellgro, Manassas, VA) containing 10% fetal bovine serum (FBS) (Sigma-Aldrich, St.Louis, MO) and 1% penicillin–streptomycin (Corning Cellgro, Manassas, VA). PSMA+ PC3 PIP cells were grown in the presence of 20 μg/mL of puromycin to maintain PSMA expression. All cell cultures were maintained in an atmosphere containing 5% carbon dioxide (CO_2), at 37.0 °C in a humidified incubator.

Cell Uptake and Internalization

Cell uptake studies were performed as previously described.[57] Cells (1 million) were incubated with 37 kBq/mL (1 μCi/mL) of each radiolabeled agent in the growth medium in 6-well plates. To determine specific uptake, cells were preblocked with ZJ43 to a final concentration of 10 μM. Cellular uptake was terminated by washing with 1 mL of ice-cold PBS. After incubation at 37 °C for 10, 30, and 60 min, cells were washed with binding

buffer, trypsinized using nonenzymatic buffer, and cell-associated activity was determined in a γ-spectrometer.

For internalization assays, cells were detached using nonenzymatic buffer, and aliquots of 1 million cells per tube were incubated with 37 kBq (1 μCi) of each radiolabeled agent per milliliter of solution for 10 min, 30 min, and 1 h at 37 °C. Assuming minimal receptor endocytosis at 4 °C, the internalization assay was performed only with cells incubated at 37 °C. At 10, 30, and 60 min intervals the medium was removed and cells were washed once with binding buffer followed by a mild acidic buffer (50 mM glycine, 150 mM NaCl [pH 3.0]) at 4 °C for 5 min. The acidic buffer was then collected and cells were washed twice with binding buffer. Pooled washes (containing cell surface-bound ^{68}Ga-labeled agent) and cell pellets (containing internalized ^{68}Ga-labeled) were counted in an automated γ-spectrometer along with the standards. All radioactivity values were converted into percentage of incubated dose (%ID) per million cells. Experiments were performed in triplicate and repeated 3 times. Data were fitted according to linear regression analysis.

Small-Animal PET Imaging and Analysis

Whole-body PET and CT images were acquired on a SuperArgus PET-CT preclinical imaging system (SEDECAL SA4R PET-CT, Madrid, Spain). For imaging studies mice were anesthetized with 3% and maintained under 1.5% isoflurane (v/v). PET-CT Imaging studies were performed on NOD/SCID mice bearing PSMA+ PC3 PIP and PSMA− PC3 flu tumors. After intravenous injection of ~150 μCi (5.55 MBq) of ^{68}**Ga-1**, ^{68}**Ga-2**, or ^{68}Ga-DKFZ-PSMA-11, whole-body PET emission images (two bed positions, 15 min per position) were acquired at the indicated (30 min, 1 h, 2 h, and 3 h) time points after injection of radiotracer.

For binding specificity studies, a mouse was subcutaneously administered a blocking dose of the known PSMA inhibitor ZJ43[37] (50 mg/kg) at 30 min before the injection of ^{68}**Ga-2**, and another mouse was injected with ^{68}**Ga-2** alone. A CT scan was acquired after each PET scan in 512 projections using a 50 keV beam for anatomic co-registration. PET emission data were corrected for decay and dead time and were reconstructed using the three-dimensional ordered-subsets expectation maximization algorithm. Data were displayed and analyzed using AMIDE software (http://sourceforge.net/amide).

Biodistribution

Mice bearing PSMA+ PC3 PIP and PSMA− PC3 flu xenografts were injected via the tail vein with 740 kBq (20 μCi) of ^{68}**Ga-1**, ^{68}**Ga-2**, and ^{68}Ga-DKFZ-PSMA-11 in 150 μL of saline (n = 4). At 1, 2, and 3 h post-injection, mice were sacrificed by cervical dislocation and the blood was immediately collected by cardiac puncture. The heart, lungs, liver, stomach, pancreas, spleen, fat, kidney, muscle, small and large intestines, urinary bladder, PSMA+ PC3 PIP, and PSMA− PC3 flu tumors were collected. Each organ was weighed, and the tissue radioactivity was measured with an automated gamma counter (1282 Compugamma CS, Pharmacia/LKBNuclear, Inc., Mt. Waverly, Victoria, Australia). The percentage of injected dose per gram of tissue (% ID/g) was calculated by comparison with samples of a standard dilution of the initial dose. All measurements were corrected for decay.

Data Analysis

Data are expressed as mean ± standard deviation (SD). Prism software (GraphPAD, San Diego, California) was used to determine statistical significance. Statistical significance was calculated using a two-tailed Student's *t* test. A *P*-value <0.05 was considered significant.

Supplementary Material

Refer to Web version on PubMed Central for supplementary material.

Acknowledgments

We are grateful to NIH K25 CA148901, U54 CA151838, R01 CA134675, R01 CA184228, U01 CA183031, and the Patrick Walsh Foundation for Prostate Cancer Research. We thank the JHU PET Center for access to the ^{68}Ga generator. We would like to thank Gilbert Green and Desmond Jacob for their assistant with imaging studies. Dr. Zhengping Chen would like to thank Jiangsu Government Scholarship for Overseas Studies (JS-2011-054) and The Key Laboratory of Nuclear Medicine, Ministry of Health, Jiangsu Institute of Nuclear Medicine, P.R. China, for his fellowship. Dr. Jian Chen would like to thank China Scholarship Council and Key Laboratory of Smart Drug Delivery, Ministry of Education and Fudan University, Shanghai, P.R. China, for his fellowship.

ABBREVIATIONS

PSMA	prostate-specific membrane antigen
PET	positron emission tomography
NOTA	1,4,7-triazacyclononane-1,4,7-triacetic acid
HBED-CC	*N,N'*-bis-[2-hydroxy-5-(carboxyethyl)benzyl]ethylenediamine-*N,N'*-diacetic acid)
DOTA-monoamide	1,4,7,10-tetraazacyclododecane-*N,N',N'',N'''*-triaacetic acid monoamide
CHX-A"-DTPA	cyclohexyl-diethylenetriaminepentaacetic acid
2-PMPA	2-phosphonomethyl pentanedioic acid

REFERENCES

1. National Cancer Institute. Cancer Statistics. 2015. http://seer.cancer.gov/statfacts/html/prost.html
2. Afshar-Oromieh A, Malcher A, Eder M, Eisenhut M, Linhart HG, Hadaschik BA, Holland-Letz T, Giesel FL, Kratochwil C, Haufe S, et al. PET imaging with a [68Ga]gallium-labelled PSMA ligand for the diagnosis of prostate cancer: biodistribution in humans and first evaluation of tumour lesions. Eur. J. Nucl. Med. Mol. Imaging. 2013; 40:486–495. [PubMed: 23179945]
3. Afshar-Oromieh A, Avtzi E, Giesel F, Holland-Letz T, Linhart H, Eder M, Eisenhut M, Boxler S, Hadaschik B, Kratochwil C, et al. The diagnostic value of PET/CT imaging with the 68Ga-labelled PSMA ligand HBED-CC in the diagnosis of recurrent prostate cancer. Eur. J. Nucl. Med. Mol. Imaging. 2015; 42:197–209. [PubMed: 25411132]
4. Murphy GP, Holmes EH, Boynton AL, Kenny GM, Ostenson RC, Erickson SJ, Barren RJ. Comparison of prostate specific antigen, prostate specific membrane antigen, and LNCaP-based enzyme-linked immunosorbent assays in prostatic cancer patients and patients with benign prostatic enlargement. Prostate. 1995; 26:164–168. [PubMed: 7534919]

5. Murphy GP, Kenny GM, Ragde H, Wolfert RL, Boynton AL, Holmes EH, Misrock SL, Bartsch G, Klocker H, Pointner J, et al. Measurement of serum prostate-specific membrane antigen, a new prognostic marker for prostate cancer. Urology. 1998; 51:89–97.
6. Murphy GP, Greene TG, Tino WT, Boynton AL, Holmes EH. Isolation and characterization of monoclonal antibodies specific for the extracellular domain of prostate specific membrane antigen. J. Urol. 1998; 160:2396–2401. [PubMed: 9817391]
7. Sweat SD, Pacelli A, Murphy GP, Bostwick DG. Prostate-specific membrane antigen expression is greatest in prostate adenocarcinoma and lymph node metastases. Urology. 1998; 52:637–640. [PubMed: 9763084]
8. Silver DA, Pellicer I, Fair WR, Heston WD, Cordon-Cardo C. Prostate-specific membrane antigen expression in normal and malignant human tissues. Clin. Cancer Res. 1997; 3:81–95. [PubMed: 9815541]
9. Wang HL, Wang SS, Song WH, Pan Y, Yu HP, Si TG, Liu Y, Cui XN, Guo Z. Expression of Prostate-Specific Membrane Antigen in Lung Cancer Cells and Tumor Neovasculature Endothelial Cells and Its Clinical Significance. PLoS One. 2015; 10:e0125924. [PubMed: 25978404]
10. Haffner MC, Kronberger IE, Ross JS, Sheehan CE, Zitt M, Muhlmann G, Ofner D, Zelger B, Ensinger C, Yang XJ, et al. Prostate-specific membrane antigen expression in the neovasculature of gastric and colorectal cancers. Hum. Pathol. 2009; 40:1754–1761. [PubMed: 19716160]
11. Haffner MC, Laimer J, Chaux A, Schafer G, Obrist P, Brunner A, Kronberger IE, Laimer K, Gurel B, Koller JB, et al. High expression of prostate-specific membrane antigen in the tumor-associated neo-vasculature is associated with worse prognosis in squamous cell carcinoma of the oral cavity. Mod. Pathol. 2012; 25:1079–1085. [PubMed: 22460809]
12. Baccala A, Sercia L, Li J, Heston W, Zhou M. Expression of prostate-specific membrane antigen in tumor-associated neovasculature of renal neoplasms. Urology. 2007; 70:385–390. [PubMed: 17826525]
13. Chang SS, Gaudin PB, Reuter VE, O'Keefe DS, Bacich DJ, Heston WD. Prostate-Specific Membrane Antigen: Much More Than a Prostate Cancer Marker. Mol. Urol. 1999; 3:313–320. [PubMed: 10851338]
14. Chang SS, O'Keefe DS, Bacich DJ, Reuter VE, Heston WD, Gaudin PB. Prostate-specific membrane antigen is produced in tumor-associated neovasculature. Clin. Cancer Res. 1999; 5:2674–2681. [PubMed: 10537328]
15. Cho SY, Gage KL, Mease RC, Senthamizhchelvan S, Holt DP, Jeffrey-Kwanisai A, Endres CJ, Dannals RF, Sgouros G, Lodge M, et al. Biodistribution, tumor detection, and radiation dosimetry of 18F–DCFBC, a low-molecular-weight inhibitor of prostate-specific membrane antigen, in patients with metastatic prostate cancer. J. Nucl. Med. 2012; 53:1883–1891. [PubMed: 23203246]
16. Afshar-Oromieh A, Haberkorn U, Eder M, Eisenhut M, Zechmann CM. [68Ga]Gallium-labelled PSMA ligand as superior PET tracer for the diagnosis of prostate cancer: comparison with 18F–FECH. Eur. J. Nucl. Med. Mol. Imaging. 2012; 39:1085–1086. [PubMed: 22310854]
17. Afshar-Oromieh A, Haberkorn U, Hadaschik B, Habl G, Eder M, Eisenhut M, Schlemmer HP, Roethke MC. PET/MRI with a 68Ga-PSMA ligand for the detection of prostate cancer. Eur. J. Nucl. Med. Mol. Imaging. 2013; 40:1629–1630. [PubMed: 23817686]
18. Afshar-Oromieh A, Haberkorn U, Schlemmer HP, Fenchel M, Eder M, Eisenhut M, Hadaschik BA, Kopp-Schneider A, Rothke M. Comparison of PET/CT and PET/MRI hybrid systems using a 68Ga-labelled PSMA ligand for the diagnosis of recurrent prostate cancer: initial experience. Eur. J. Nucl. Med. Mol. Imaging. 2014; 41:887–897. [PubMed: 24352789]
19. Eiber M, Maurer T, Kubler H, Gschwend JE, Souvatzoglou M, Ruffani A, Graner F-P, Schwaiger M, Beer AJ, Haller B, Haberhorn U, Eisenhut M, Wester H-J. Evaluation of Hybrid 68Ga-PSMA Ligand PET/CT in 248 Patients with Biochemical Recurrence After Radical Prostatectomy. J. Nucl. Med. 2015; 56:668–674. [PubMed: 25791990]
20. Eiber M, Nekolla SG, Maurer T, Weirich G, Wester H-J, Schwaiger M. 68)Ga-PSMA PET/MR with multimodality image analysis for primary prostate cancer. Abdominal Imaging. 2015; 40:1769–1771. [PubMed: 25412869]
21. Rowe SP, Gage KL, Faraj SF, Macura KJ, Cornish TC, Gonzalez-Roibon N, Guner G, Munari E, Partin AW, Pavlovich CP, Han M, Carter HB, Bivalacqua TJ, Blackford A, Holt D, Dannals RF,

Netto GJ, Lodge MA, Mease RC, Pomper MG, Cho SY. 18F-DCFBC PET/CT for PSMA-Based Detection and Characterization of Primary Prostate Cancer. J. Nucl. Med. 2015; 56:1003–1010. [PubMed: 26069305]

22. Fani M, Andre JP, Maecke HR. 68Ga-PET: a powerful generator-based alternative to cyclotron-based PET radio-pharmaceuticals. Contrast Media Mol. Imaging. 2008; 3:53–63. [PubMed: 18383455]
23. Banerjee SR, Pullambhatla M, Byun Y, Nimmagadda S, Green G, Fox JJ, Horti A, Mease RC, Pomper MG. 68Ga-labeled inhibitors of prostate-specific membrane antigen (PSMA) for imaging prostate cancer. J. Med. Chem. 2010; 53:5333–5341. [PubMed: 20568777]
24. Eder M, Schafer M, Bauder-Wust U, Hull WE, Wangler C, Mier W, Haberkorn U, Eisenhut M. 68Ga-complex lipophilicity and the targeting property of a urea-based PSMA inhibitor for PET imaging. Bioconjugate Chem. 2012; 23:688–697.
25. Weineisen M, Simecek J, Schottelius M, Schwaiger M, Wester H-J. Synthesis and preclinical evaluation of DOTAGA-conjugated PSMA ligands for functional imaging and endoradiotherapy of prostate cancer. EJNMMI Res. 2014; 4:1–15. [PubMed: 24382020]
26. Weineisen M, Schottelius M, Simecek J, Baum RP, Yildiz A, Beykan S, Kulkarni HR, Lassmann M, Klette I, Eiber M, et al. 68Ga- and 177Lu-labeled PSMA I&T: Optimization of a PSMA targeted theranostic concept and first proof of concept human studies. J. Nucl. Med. 2015; 56:1169–1176. [PubMed: 26089548]
27. Herrmann K, Bluemel C, Weineisen M, Schottelius M, Wester HJ, Czernin J, Eberlein U, Beykan S, Lapa C, Riedmiller H, Krebs M, Kropf S, Schirbel A, Buck AK, Lassmann M. Biodistribution and radiation dosimetry for a probe targeting prostate-specific membrane antigen for imaging and therapy. J. Nucl. Med. 2015; 56:855–861. [PubMed: 25883128]
28. Reske SN, Winter G, Baur B, Machulla HJ, Kull T. Comment on Afshar-Oromieh et al.: PET imaging with a [68Ga]gallium-labelled PSMA ligand for the diagnosis of prostate cancer: biodistribution in humans and first evaluation of tumour lesions. Eur. J. Nucl. Med. Mol. Imaging. 2013; 40:969–970. [PubMed: 23558687]
29. Baur B, Solbach C, Andreolli E, Winter G, Machulla HJ, Reske SN. Synthesis, radiolabelling and in vitro characterization of the Gallium-68-, Yttrium-90- and Lutetium-177-Labelled PSMA Ligand, CHX-A”-DTPA-DUPA-Pep. Pharmaceuticals. 2014; 7:517–529. [PubMed: 24787458]
30. Afshar-Oromieh A, Malcher A, Eder M, Eisenhut M, Linhart HG, Hadaschik BA, Holland-Letz T, Giesel FL, Kratochwil C, Haufe S, et al. Reply to Reske et al.: PET imaging with a [68Ga]gallium-labelled PSMA ligand for the diagnosis of prostate cancer: biodistribution in humans and first evaluation of tumour lesions. Eur. J. Nucl. Med. Mol. Imaging. 2013; 40:971–972. [PubMed: 23558688]
31. Mottaghy F, Behrendt F, Verburg F. 68Ga-PSMA-HBED-CC PET/CT: where molecular imaging has an edge over morphological imaging. Eur. J. Nucl. Med. Mol. Imaging. 2016; 43:394–396. [PubMed: 26452581]
32. Broan CJ, COX JPL, Craig AS, Kataky R, Parker D, Harrison A, Randall AM, Ferguson G. Structure and solution stability of indium and gallium complexes of 1,4,7-Triazacyclononanetriacetate and of yttrium complexes of 1,4,7,1 O-tetraazacyclododecanetetraacetate and related ligands: kinetically stable complexes for use in imaging and radioimmunotherapy. X-Ray molecular structure of the Indium and gallium complexes of 1,4,7-Triazacyclononane-I, 4,7-triacetic Acid. J. Chem. Soc., Perkin Trans. 1991; 2:87–99.
33. Eplattenier FL, Murase I, Martell AE. New Multidentate Ligands. VI. Chelating Tendencies of N,N-Di (2-hydroxybenzyl) ethylenediamine-N,N-diacetic Acid. J. Am. Chem. Soc. 1967; 89:837–843.
34. Zöller M, Schuhmacher J, Reed J, Maier-Borst W, Matzku S. Establishment and Characterization of Monoclonal Antibodies Against an Octahedral Gallium Chelate Suitable for Immunoscintigraphy with PET. J. Nucl. Med. 1992; 33:1366–1372. [PubMed: 1613579]
35. Eder M, Wängler B, Knackmuss S, LeGall F, Little M, Haberkorn U, Mier W, Eisenhut M. Tetrafluorophenolate of HBED-CC: a versatile conjugation agent for 68Ga-labeled small recombinant antibodies. Eur. J. Nucl. Med. Mol. Imaging. 2008; 35:1878–1886. [PubMed: 18509635]

36. Zhernosekov KP, Filosofov DV, Baum RP, Aschoff P, Bihl H, Razbash AA, Jahn M, Jennewein M, Rosch F. Processing of generator-produced 68Ga for medical application. J. Nucl. Med. 2007; 48:1741–1748. [PubMed: 17873136]
37. Olszewski RT, Bukhari N, Zhou J, Kozikowski AP, Wroblewski JT, Shamimi-Noori S, Wroblewska B, Bzdega T, Vicini S, Barton FB, Neale JH. NAAG peptidase inhibition reduces locomotor activity and some stereotypes in the PCP model of schizophrenia via group II mGluR. J. Neurochem. 2004; 89:876–885. [PubMed: 15140187]
38. Banerjee SR, Foss CA, Castanares M, Mease RC, Byun Y, Fox JJ, Hilton J, Lupold SE, Kozikowski AP, Pomper MG. Synthesis and evaluation of technetium-99m- and rhenium-labeled inhibitors of the prostate-specific membrane antigen (PSMA). J. Med. Chem. 2008; 51:4504–4517. [PubMed: 18637669]
39. Kularatne SA, Wang K, Santhapuram H-KR, Low PS. Prostate-specific membrane antigen targeted imaging and therapy of prostate cancer using a PSMA inhibitor as a homing ligand. Mol. Pharmaceutics. 2009; 6:780–789.
40. Kularatne SA, Zhou Z, Yang J, Post CB, Low PS. Design, synthesis, and preclinical evaluation of prostate-specific membrane antigen targeted (99m)Tc-radioimaging agents. Mol. Pharmaceutics. 2009; 6:790–800.
41. Zhang AX, Murelli RP, Barinka C, Michel J, Cocleaza A, Jorgensen WL, Lubkowski J, Spiegel DA. A remote arene-binding site on prostate specific membrane antigen revealed by antibody-recruiting small molecules. J. Am. Chem. Soc. 2010; 132:12711–12716. [PubMed: 20726553]
42. Nedrow-Byers JR, Jabbes M, Jewett C, Ganguly T, He H, Liu T, Benny P, Bryan JN, Berkman CE. A phosphoramidate-based prostate-specific membrane antigen-targeted SPECT agent. Prostate. 2012; 72:904–912. [PubMed: 22670265]
43. Nedrow-Byers JR, Moore AL, Ganguly T, Hopkins MR, Fulton MD, Benny PD, Berkman CE. PSMA-targeted SPECT agents: mode of binding effect on in vitro performance. Prostate. 2013; 73:355–362. [PubMed: 22911263]
44. Nguyen QT, Tsien RY. Fluorescence-guided surgery with live molecular navigation-a new cutting edge. Nat. Rev. Cancer. 2013; 13:653–662. [PubMed: 23924645]
45. Ray Banerjee S, Pullambhatla M, Foss CA, Falk A, Byun Y, Nimmagadda S, Mease RC, Pomper MG. Effect of chelators on the pharmacokinetics of (99m)Tc-labeled imaging agents for the prostate-specific membrane antigen (PSMA). J. Med. Chem. 2013; 56:6108–6121. [PubMed: 23799782]
46. Banerjee SR, Pullambhatla M, Foss CA, Nimmagadda S, Ferdani R, Anderson CJ, Mease RC, Pomper MG. 6)(4)Cu-labeled inhibitors of prostate-specific membrane antigen for PET imaging of prostate cancer. J. Med. Chem. 2014; 57:2657–2669. [PubMed: 24533799]
47. Benesova M, Schafer M, Bauder-Wust U, Afshar-Oromieh A, Kratochwil C, Mier W, Haberkorn U, Kopka K, Eder M. Preclinical Evaluation of a Tailor-Made DOTA-Conjugated PSMA Inhibitor with Optimized Linker Moiety for Imaging and Endoradiotherapy of Prostate Cancer. J. Nucl. Med. 2015; 56:914–920. [PubMed: 25883127]
48. Banerjee SR, Foss CA, Pullambhatla M, Wang Y, Srinivasan S, Hobbs RF, Baidoo KE, Brechbiel MW, Nimmagadda S, Mease RC, et al. Preclinical evaluation of 86Y–labeled inhibitors of prostate-specific membrane antigen for dosimetry estimates. J. Nucl. Med. 2015; 56:628–634. [PubMed: 25722448]
49. Studer M, Meares CF. Synthesis of novel 1,4,7-triazacyclononane-N,N′,N″-triacetic acid derivatives suitable for protein labeling. Bioconjugate Chem. 1992; 3:337–341.
50. Roesch F, Riss PJ. The renaissance of the (6) (8)Ge/(6)(8)Ga radionuclide generator initiates new developments in (6)(8)Ga radiopharmaceutical chemistry. Curr. Top. Med. Chem. 2010; 10:1633–1668. [PubMed: 20583984]
51. Banerjee SR, Pullambhatla M, Byun Y, Nimmagadda S, Foss CA, Green G, Fox JJ, Lupold SE, Mease RC, Pomper MG. Sequential SPECT and optical imaging of experimental models of prostate cancer with a dual modality inhibitor of the prostate-specific membrane antigen. Angew. Chem., Int. Ed. 2011; 50:9167–9170.

52. Banerjee SR, Pullambhatla M, Shallal H, Lisok A, Mease RC, Pomper MG. A modular strategy to prepare multivalent inhibitors of prostate-specific membrane antigen (PSMA). Oncotarget. 2011; 2:1244–1253. [PubMed: 22207391]

53. Nedrow JR, Latoche JD, Day KE, Modi J, Ganguly T, Zeng D, Kurland BF, Berkman CE, Anderson CJ. Targeting PSMA with a Cu-64 labeled phosphoramidate inhibitor for PET/CT Imaging of variant PSMA-expressing xenografts in mouse models of prostate cancer. Mol. Imaging Biol. 2015; 11:1–9.

54. Dumont RA, Deininger F, Haubner R, Maecke HR, Weber WA, Fani M. Novel (64)Cu- and (68)Ga-labeled RGD conjugates show improved PET imaging of alpha(nu)beta(3) integrin expression and facile radiosynthesis. J. Nucl. Med. 2011; 52:1276–1284. [PubMed: 21764795]

55. Fani M, Del Pozzo L, Abiraj K, Mansi R, Tamma ML, Cescato R, Waser B, Weber WA, Reubi JC, Maecke HR. PET of somatostatin receptor-positive tumors using 64Cu- and 68Ga-somatostatin antagonists: the chelate makes the difference. J. Nucl. Med. 2011; 52:1110–1118. [PubMed: 21680701]

56. Cheng Y, Prusoff WH. Relationship between the inhibition constant (K1) and the concentration of inhibitor which causes 50% inhibition (I50) of an enzymatic reaction. Biochem. Pharmacol. 1973; 22:3099–3108. [PubMed: 4202581]

57. De Silva RA, Peyre K, Pullambhatla M, Fox JJ, Pomper MG, Nimmagadda S. Imaging CXCR4 expression in human cancer xenografts: evaluation of monocyclam 64Cu-AMD3465. J. Nucl. Med. 2011; 52:986–993. [PubMed: 21622896]

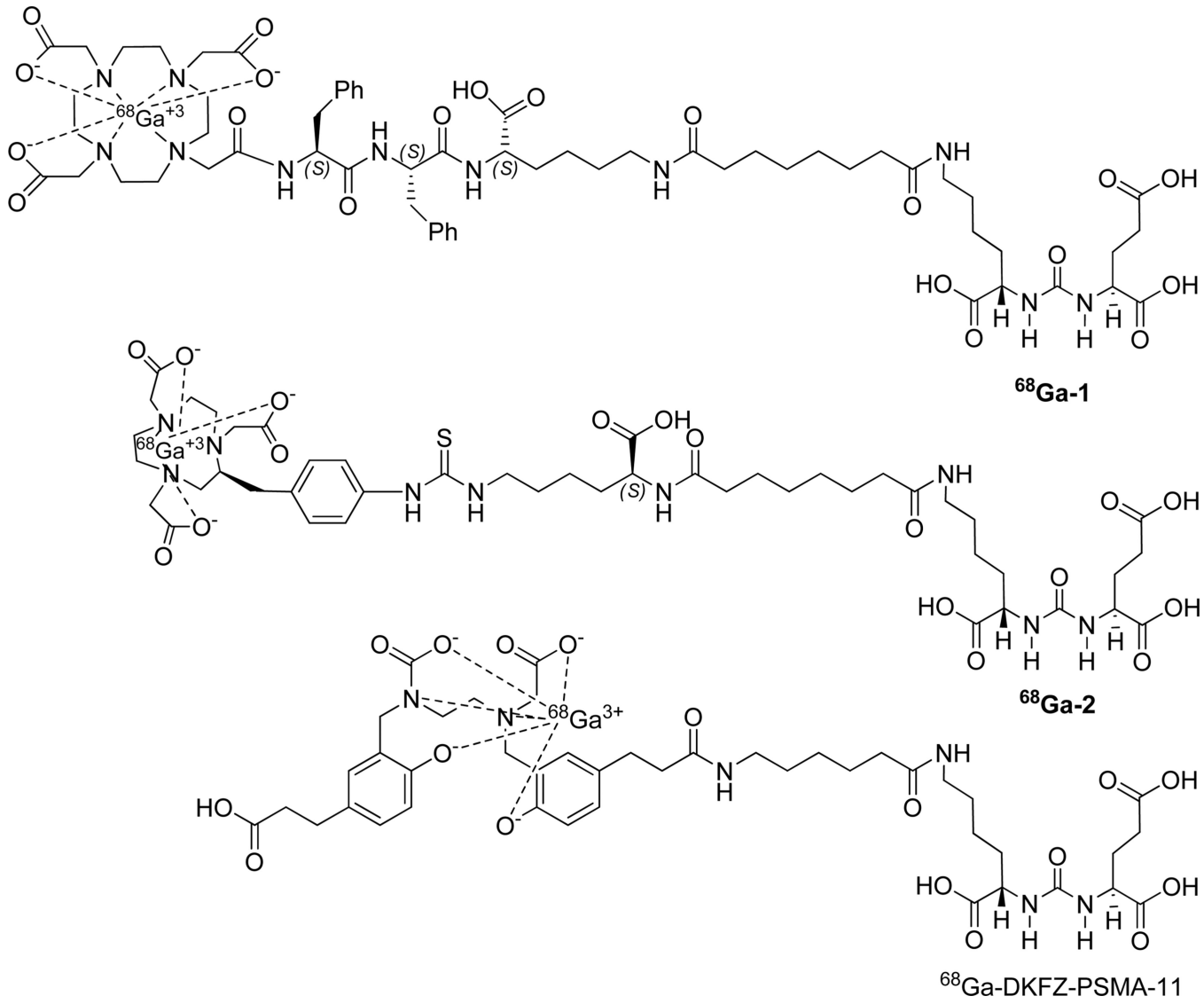

Figure 1.
Structure of ^{68}Ga-labeled PSMA inhibitors.

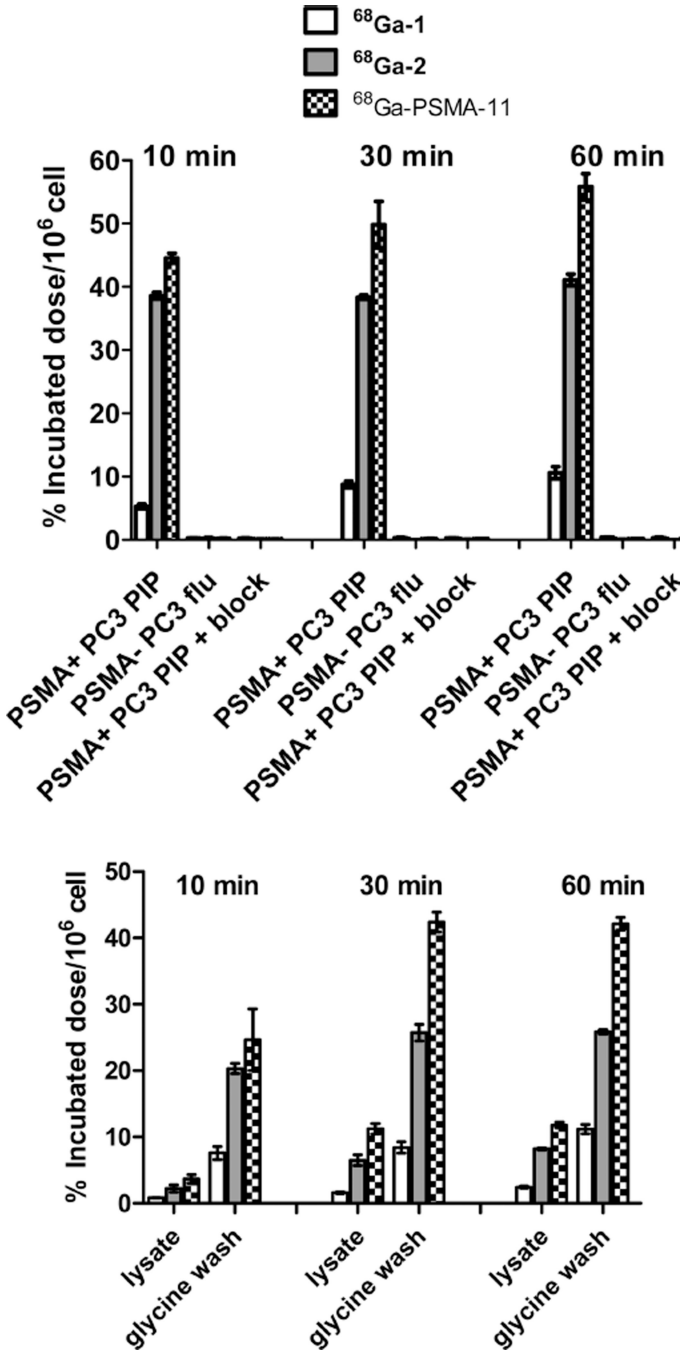

Figure 2.

(Top) PSMA+ PC3 PIP and PSMA− PC3 flu cell binding for ^{68}**Ga-1**, ^{68}**Ga-2**, and ^{68}Ga-PSMA-11 and blocking studies of the agents in PSMA+ PC3 PIP cell after 10 min of preincubation in the presence ZJ43 (10 μM). (Bottom) Internalization studies at 37 °C in PSMA+ PC3 PIP cells at 10, 30, and 60 min post-incubation. Values are calculated as percentage of incubated radioactivity dose bound to 10^6 cells. Data are expressed as mean ± SD (n = 3).

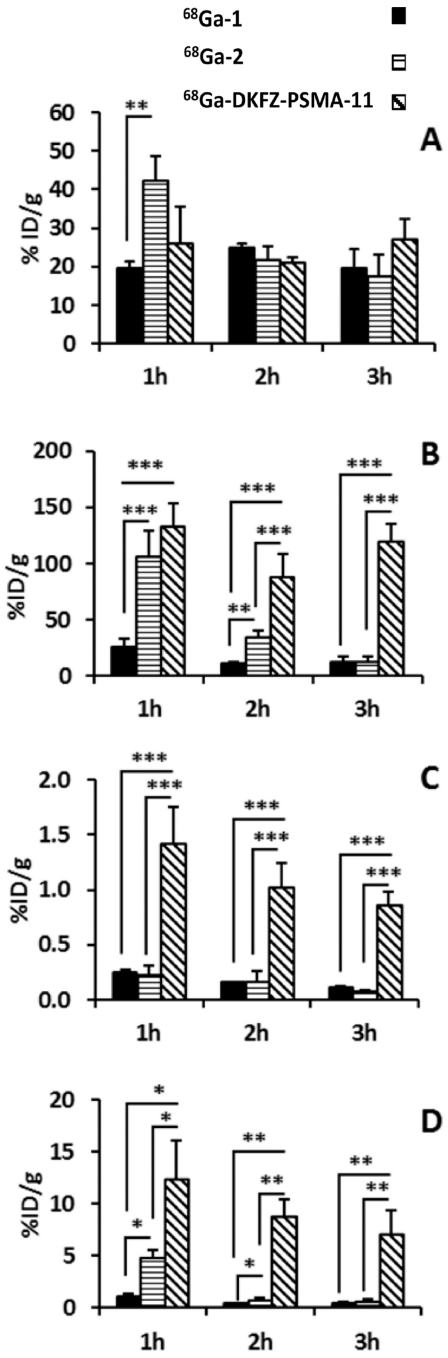

Figure 3.

Comparison of selected tissue uptake of ^{68}**Ga-1**, ^{68}**Ga-2**, and ^{68}Ga-DKFZ-PSMA-11 in male SCID-NOD mice ($n = 4$) bearing both PSMA+ PC3 PIP and PSMA− PC3 flu tumors: (A) PSMA+ PC3 PIP tumor; (B) kidney; (C) salivary gland; and (D) spleen. (*, $P < 0.05$; **, $P < 0.01$; ***, $P < 0.001$).

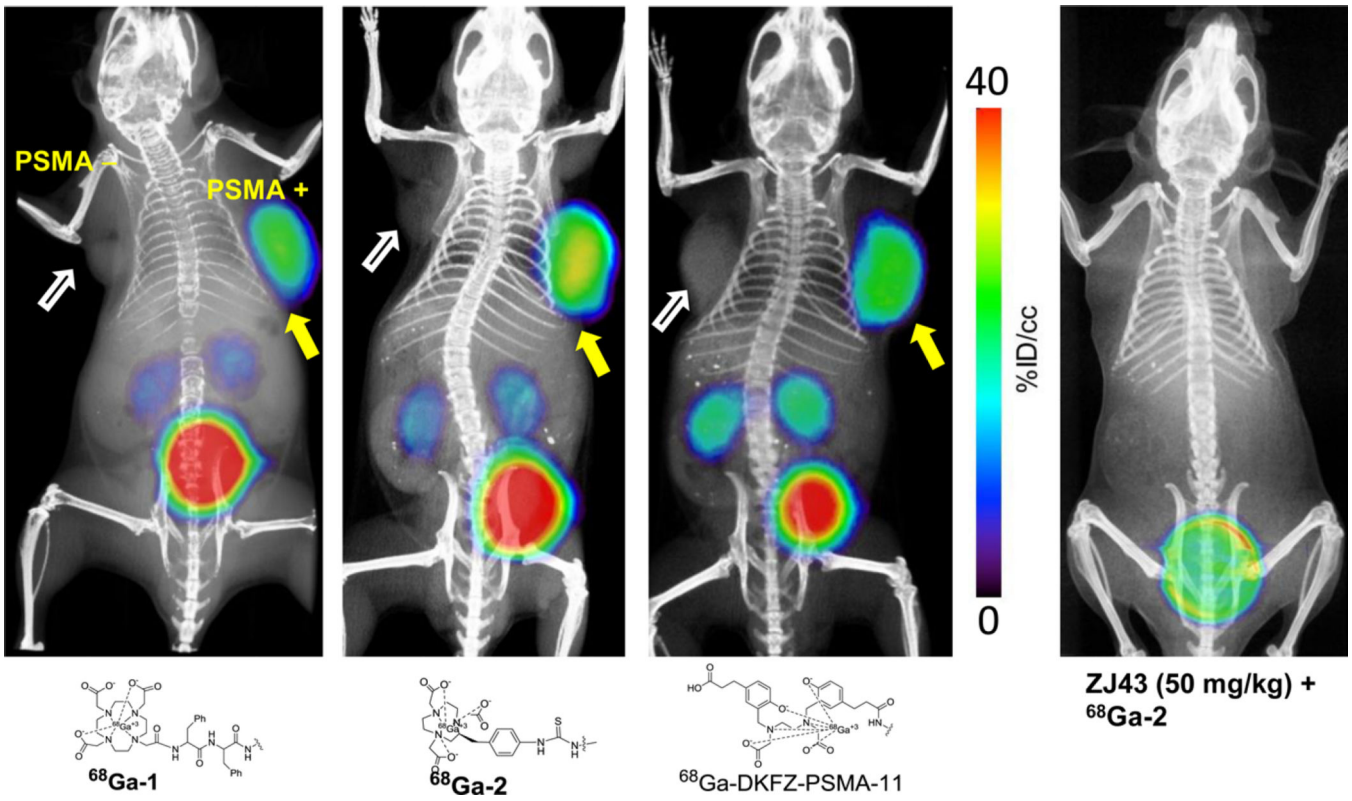

Figure 4.

PET-CT images of ^{68}**Ga-1**, ^{68}**Ga-2**, and ^{68}Ga-DKFZ-PSMA-11 at 1 h post-injection using NOD-SCID male mice bearing both PSMA+ PC3 PIP (right) and PSMA− flu (left) tumor xenografts within the upper flanks. PSMA+ PC3 tumor uptake for ^{68}**Ga-2** was further blocked by injecting ZJ43 (50 mg/kg), 30 min prior to injection of the radiotracer.

Table 1

Selected Physical Properties of Compounds Studied[a]

	molar mass (g/mol)	K_i (nM)	95% CI of K_i (nM)	HPLC (RP) retention time (min)
1	1284.4	0.70	0.42–1.16	19.2–19.8[b]
Ga-1	1352.5	0.33	0.17–0.66	26.8–31.7[b]
2	1054.2	0.81	0.35–1.89	23.9–24.9[c]
Ga-2	1120.9	0.38	2.26–6.28	20.8–22.5[c]
DKFZ-PSMA-11	947.0	0.03	0.016–0.06	34.5–40.0[c]
Ga-DKFZ-PSMA-11	1013.7	N.A.	N.A.	14.5–20.0[c]
ZJ43	304.3	0.31	0.20–0.48	N.A.

[a] Compounds **1** and **2** are the unlabeled compounds containing DOTA-monoamide and NOTA-Bn-SCN chelating agents, respectively.

[b] Isocratic solution of 80% A and 20% B.

[c] Isocratic solution of 85% water and 15% B. Flow rate was 1 mL/min for both methods.

Table 2

Tissue Biodistribution of ^{68}**Ga-1**, ^{68}**Ga-2**, and ^{68}Ga-DKFZ-PSMA-11 in Mice Bearing PSMA+ PC3 PIP and PSMA-PC3 Flu Tumors ($n = 4$)[a]

	^{68}Ga-1			^{68}Ga-2			^{68}Ga-DKFZ-PSMA-11		
tissue	**1 h**	**2 h**	**3 h**	**1 h**	**2 h**	**3 h**	**1 h**	**2 h**	**3 h**
blood	0.5 ± 0.1	0.3 ± 0.0	0.2 ± 0.0	0.4 ± 0.2	0.1 ± 0.0	0.1 ± 0.0	0.8 ± 0.2	0.4 ± 0.1	0.3 ± 0.1
heart	0.2 ± 0.0	0.1 ± 0.0	0.1 ± 0.0	0.2 ± 0.1	0.0 ± 0.0	0.0 ± 0.0	0.4 ± 0.2	0.3 ± 0.1	0.2 ± 0.0
lung	0.4 ± 0.0	0.2 ± 0.0	0.1 ± 0.0	1.0 ± 0.2	0.3 ± 0.0	0.2 ± 0.1	2.2 ± 0.5	2.1 ± 0.7	1.3 ± 0.2
liver	0.2 ± 0.0	0.2 ± 0.0	0.1 ± 0.0	0.5 ± 0.2	0.2 ± 0.0	0.2 ± 0.0	0.8 ± 0.2	0.3 ± 0.1	0.4 ± 0.2
spleen	1.0 ± 0.3	0.4 ± 0.0	0.4 ± 0.2	4.9 ± 0.7	0.8 ± 0.2	0.7 ± 0.1	12.4 ± 3.8	8.9 ± 1.5	7.2 ± 2.3
kidney	26.5 ± 6.9	11.9 ± 1.0	12.1 ± 5.6	106 ± 23	34.7 ± 5.7	12.7 ± 4.9	133 ± 21	89 ± 20	120 ± 16
muscle	0.1 ± 0.1	0.0 ± 0.0	0.0 ± 0.0	0.1 ± 0.0	0.0 ± 0.0	0.0 ± 0.0	0.3 ± 0.1	0.2 ± 0.1	0.1 ± 0.0
small intestine	0.2 ± 0.0	0.1 ± 0.0	0.1 ± 0.0	0.2 ± 0.1	0.0 ± 0.0	0.1 ± 0.0	0.4 ± 0.1	0.2 ± 0.1	0.2 ± 0.1
salivary gland	0.3 ± 0.0	0.2 ± 0.0	0.1 ± 0.0	0.2 ± 0.1	0.2 ± 0.1	0.1 ± 0.0	1.4 ± 0.3	1.0 ± 0.2	0.9 ± 0.1
PSMA+ PC3 PIP	19.5 ± 1.8	24.8 ± 1.1	19.5 ± 5.1	42.2 ± 6.7	21.7 ± 3.7	17.4 ± 5.6	26.0 ± 9.7	21.1 ± 1.2	26.9 ± 5.6
PSMA− PC3 flu	0.2 ± 0.0	0.2 ± 0.0	0.2 ± 0.0	0.4 ± 0.1	0.10 ± 0.0	0.1 ± 0.0	0.6 ± 0.1	0.4 ± 0.2	0.3 ± 0.1
PIP:flu	84 ± 4	149 ± 16	122 ± 31	110 ± 22	232 ± 26	182 ± 15	47 ± 8	58 ± 27	111 ± 21
PIP:kidney	0.8 ± 0.3	2.1 ± 0.1	1.8 ± 0.6	0.4 ± 0.1	0.7 ± 0.1	1.6 ± 0.1	0.2 ± 0.1	0.2 ± 0.0	0.2 ± 0.0
PIP:blood	59 ± 25	101 ± 10	236 ± 24	120 ± 29	321 ± 79	207 ± 33	36 ± 13	52 ± 11	80 ± 10
PIP:salivary gland	77 ± 3	157 ± 3	173 ± 27	188 ± 35	212 ± 3	222 ± 35	18.6 ± 9.0	21 ± 3	31 ± 5

[a]Values are expressed as mean ± SD.